

Abdullah G. Al-Sehemi, Ahmed Irfan, Mehboobali Pannipara*,
Mohammed A. Assiri and Abul Kalam

Anthracene Based AIE Active Probe for Colorimetric and Fluorimetric Detection of Cu^{2+} Ions

<https://doi.org/10.1515/zpch-2018-1215>

Received April 23, 2018; accepted October 10, 2018

Abstract: A novel aggregation induced emission (AIE) active anthracene based dihydroquinazolinone derivative (probe **1**) has been synthesized and characterized by means of spectroscopic methods. The photophysical properties of this probe have been investigated in solvents of different polarity display that fluorescence states are of intramolecular charge transfer (ICT) character. Probe **1** show clear AIE behavior in water/THF mixture on reaching water fraction 95%. The AIE behavior of probe **1** have been exploited for the detection of metal ions in aqueous solution which reveals high selectivity and sensitivity towards Cu^{2+} ions by colorimetrically and function as a chemosensor in a remarkable turn-off fluorescence manner. Further, the experimental results were investigated by computational means by optimizing the ground state geometries of probe **1** and probe **1**-Cu complex using density functional theory (DFT) at B3LYP/6-31G** and B3LYP/6-31G** (LANL2DZ) levels of theory. Intra-molecular charge transfer was observed in probe **1** while ligand to metal charge transfer (LMCT) for probe **1**-Cu complex.

Keywords: AIE active; anthracene; Cu^{2+} ions

***Corresponding author: Mehboobali Pannipara**, Department of Chemistry, Faculty of Science, King Khalid University, P.O. Box 9004, Abha 61413, Saudi Arabia; and Research Center for Advanced Materials Science (RCAMS), King Khalid University, P.O. Box 9004, Abha 61413, Saudi Arabia, Tel.: +966 553956503, Fax: +0096672418426, e-mail: mpannipara@kku.edu.sa, mhbb25@gmail.com

Abdullah G. Al-Sehemi, Ahmed Irfan, Mohammed A. Assiri and Abul Kalam: Department of Chemistry, Faculty of Science, King Khalid University, P.O. Box 9004, Abha 61413, Saudi Arabia; and Research Center for Advanced Materials Science (RCAMS), King Khalid University, P.O. Box 9004, Abha 61413, Saudi Arabia

1 Introduction

Design and fabrication of stimuli responsive organic fluorescent materials have been receiving tremendous attention in recent years in the field of science and technology as its optical properties can be tuned for numerous applications such as sensors, displays, switches, security inks, and optoelectronic devices [1–4]. The tunable optical and electrical properties of these π -conjugated molecules for such applications arise from the non-covalent interaction associated with molecular packing or self-assembly of molecules in the condensed state [5]. Hence, developing such high performance smart switching materials with desirable photophysical properties could be achieved by altering the molecular packing of the fluorophore by controlling the intermolecular interactions [6].

Fluorescence based molecular probes has witnessed a tremendous growth over the last decades for the selective and sensitive detection of heavy metal ions as the method of operation is rapid, convenient and simple [7, 8]. Stimuli responsive molecular material are considered to be ideal candidates for the use for chemical sensor as the change in molecular configuration brought out by the external stimulus or analyte can be detected either by colorimetric or fluorimetric approach [9, 10]. Compared with the procedures based on expensive equipment, sensing of metals with the help of easily synthesized receptor and nominal instrumental support with the help of small organic molecule-derived probes established on color or fluorescence changes has the benefits of low cost, high sensitivity and appropriate operation. A colorimetric probe will stimulate color changes on addition of the target ion which can be observed by the naked eyes. A fluorometer or even a portable UV lamp can be used to analyze the fluorescent changes imparted by fluorescent probes [11]. Designing and developing such a probe involves linking a recognition unit to signal reporting chromophore that can act as efficient binding site [12].

The explorations of novel AIE-active materials are currently attracting significant attention especially for to design the ligands having selective and significant binding abilities towards various metal ions. The toxic effects of heavy metal ions in the environment have been well-documented, and a large number of selective and sensitive sensors for the determination of heavy metals in varying chemical systems have been continually devised. Among them, AIE-active molecular switches with multi-stimuli-responsive features with potential binding units such as SH, OH, and NH towards various metal ions are currently attracting significant attention for to design the ligands for the selective and significant detection in a broad range of environments [13, 14]. Recently, we have reported AIE active Schiff base derivative fluorescent probes for the rapid detection of Cu^{2+} ions via

a simple and effective method [15]. AIE-active fluorescent probes, as compared to other fluorescent probes that are available in the literature for sensing mostly work only in organic solvents, enjoy great advantages as it mostly works in aqueous media as water is responsible for aggregation in most cases and the detection limit is too low. The current work report on the photophysical properties of an AIE active anthracene appended dihydroquinazolinone derivative (probe **1**). The AIE behavior of probe **1** was further exploited for the selective and sensitive determination of Cu^{2+} ions through remarkable turn-off fluorescence manner colorimetric response towards Cu^{2+} along with colorimetric response under physiological conditions.

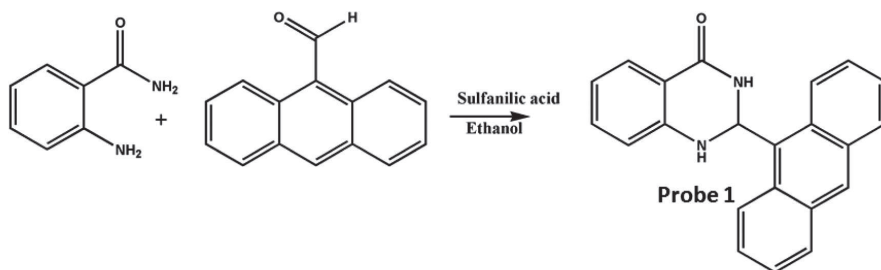
2 Experimental

2.1 Materials and methods

Analytical grade chemicals and solvents used in this study were used without further purification. Reaction was monitored by thin layer chromatography (TLC) with the aid of UV light. 2-amino benzamide, 9-Anthracenecarboxaldehyde, sulfanilic acid and metal salts were purchased from Sigma–Aldrich and Merck. Stock solution of the title compound and its dilutions were prepared for UV–visible and fluorescent study at different concentrations. Stock solutions of the salts of Ag^+ , Co^{2+} , Cu^{2+} , Ni^{2+} , Hg^{2+} , Zn^{2+} , Mn^{2+} , Cd^{2+} and Pb^{2+} were prepared in distilled water and test solutions for metal ion detection were prepared by diluting appropriate aliquot of each metal ion stock and compound stock solution to desired concentration. Twenty micromole solutions of probe **1** in THF or water/THF mixtures with different water fractions were prepared to analyze the AIE characteristics.

2.2 Spectral measurements

Gallenkamp melting point apparatus was used to determine the melting point and the infrared (IR) spectra were recorded on Shimadzu FT-IR 8400S infrared spectrophotometer using KBr pellets. The NMR (^1H and ^{13}C) spectra were recorded on a Bruker DPX-600 at 600 MHz and 150 MHz, respectively, using TMS as the internal standard. The chemical shift values are documented on δ scale and coupling constants (J) in Hertz; Splitting patterns were entitled as follows: *s*: singlet; *d*: doublet; *m*: multiplet. PG UV-160A spectrophotometer was used to record the UV-Vis electronic absorption spectra, and the steady-state fluorescence spectra were



Scheme 1: Synthetic route for probe 1.

measured using Varain Cary Eclipse spectrofluorophotometer using a rectangular quartz cell of dimensions 0.2 cm \times 1 cm.

2.3 Synthetic procedure for probe 1

Probe 1 was synthesized by the sulfanilic acid catalyzed reaction between 2-amino benzamide and 9-Anthracenecarboxaldehyde in aqueous ethanol (Scheme 1) [15]. A mixture of 2-amino benzamide (10 mmol), 9-Anthracenecarboxaldehyde (10 mmol) and sulfanilic acid (1 mmol) in 50% aq ethanol (25 mL) was stirred at 70 °C and the reaction progress was monitored by TLC. After the completion of the reaction as indicated from TLC, the reaction mass was allowed stand overnight at room temperature. The obtained product was collected by simple filtration and washed with 50% aqueous ethanol and purified by crystallization using aqueous ethanol to get the product as off green solid. The structure of the compound was confirmed by IR, ^1H NMR and ^{13}C NMR. Melting point: 202–204 °C; ^1H -NMR (600 MHz, d_6 -DMSO) δ : 4.18 (s, 1H, NH), 6.61 (d, 1H), 6.76 (dd, 1H), 7.29 (dd, 1H), 7.35 (dd, 1H), 7.36 (dd, 1H), 7.38 (dd, 1H), 7.4 (dd, 1H), 7.73 (d, 1H), 7.80 (d, 1H), 7.8 (d, 1H), 7.82 (d, 1H), 7.90 (1H, d), 8.10 (s, 1H), 8.20 (s, 1H, NH); ^{13}C -NMR (150 MHz, d_6 -DMSO) δ : 65.35, 112.33, 116.72, 124.49, 124.74, 125, 125.2, 125.8, 126.74, 128.2, 128.62, 128.70, 131.56, 132.30, 132.72, 132.3, 132.2, 134.2, 143.6, 168.42; FT-IR (KBr) (cm^{-1}): 2950–3300, 1730.2, 1139.9, 1197.1, 1250.9, 1289.82, 1365.58, 1448.9.

3 Results and discussion

3.1 Photophysical and aggregation-induced emission properties

The solvent effect on the photophysical properties of probe 1 (20 μM) has been elucidated by applying UV-vis absorption and emission measurements. As inferred

from Figure 1a, absorption spectra show typical features of anthracene chromophore with characteristic vibronic patterns between 350 and 390 nm corresponding to the $\pi-\pi^*$ transition without any shift in the spectra on changing the polarity of the solvents which rules out the possibility of charge transfer character in the ground state. As seen in Figure 1b, emission spectra of probe **1** is found to be markedly influenced by the polarity of the solvents. On exciting at 365 nm, it shows more structured emission spectra in aprotic solvents with significant emission intensity which may arise due to attainment of more coplanar structure during excitation whereas weakened light emission with significant red

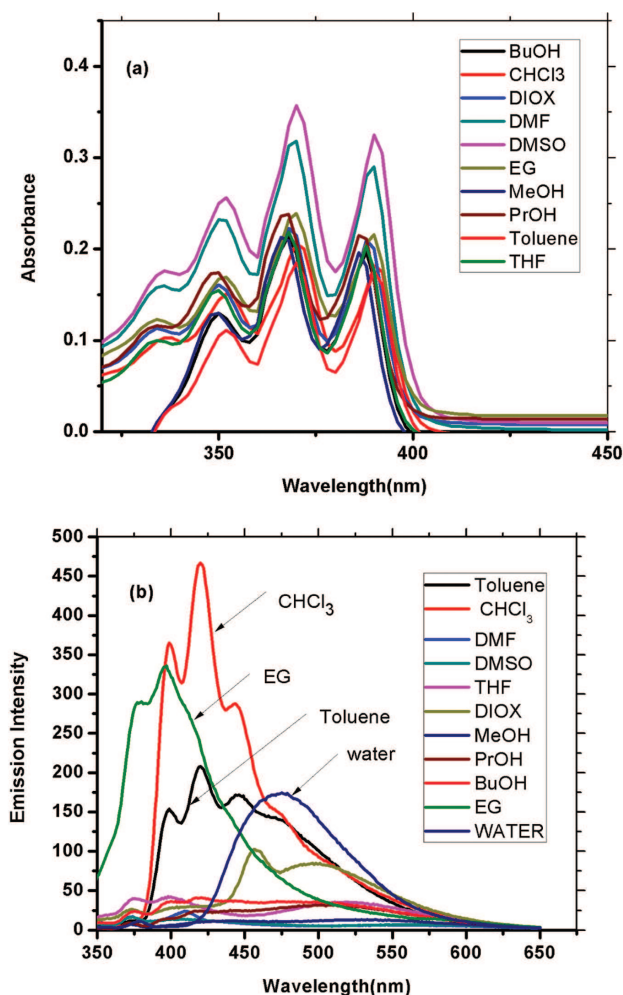


Fig. 1: Electronic absorption spectra (a) and emission spectra (b) of receptor **1** (20 μ M) in different solvents.

shift is observed on increasing polarity of solvents suggesting involvement of photo induced intramolecular charge transfer (ICT) in the excited state [16]. The emission intensity of probe **1** in dramatically decreases on increasing the solvent polarity with disappearance of its vibrational structure, which could be attributed to the specific solute solvent interaction such as hydrogen bonding or due to the stabilization of the twisted intramolecular charge transfer (TICT) state by the solvating effect of the polar solvents [17]. However, it is interesting note that, an exception for this general trend was observed in the case of ethylene glycol and water. The emission profile of ethylene glycol is slightly blue shifted ~ 24 nm from that of toluene with significant emission enhancement and somewhat structured band, whereas a broad red shifted (56 nm) band with remarkable emission intensity was observed in case of water. The slight blue shift in ethylene glycol with fine structure could easily be explained in terms of high viscosity of the solvent in which the emission arises from the state close to Franck-Condon state as observed in the case of nonpolar solvents due to restriction of intramolecular rotation that hinder the TICT state by favoring the planar aggregated state [18]. Though probe **1** is non fluorescent in alcoholic solvents, it emits strongly in water, ethylene glycol and in solid state suggesting the presence of aggregation induced (AIE) character.

Generally, the aggregated state of compounds was brought about by dissolving it in pure solvent and then adding incremental amount of a poor solvent. Herein, the AIE characteristics of probe **1** were investigated by dissolving it in pure THF and then adding different volumes of water fractions (f_w , vol %) from 0 to 98% by keeping the probe concentration fixed (20 μM). Figure 2 represents the photographic images of probe **1** (20 μM) at different THF-water mixture systems taken under UV 365 nm illumination and the corresponding absorption and emission spectra recorded at selected increment of water fraction (f_w) are shown in Figures 3 and 4. These figures clearly demonstrate AIE behavior of probe **1**. As evident from Figure 3, increasing water fractions have profound effect on the absorption spectra of probe **1**. Absorbance of probe **1** remains unchanged up to the water fractions 90%, but a decrease in absorbance was observed on further addition of the water fractions accompanied by the appearance of level-off tails at higher wavelength region that could be attributed to the well-known Mei scattering effect, which has been well documented in the literatures for AIE-active molecules [19]. The reduction in absorbance at higher water fraction ($f_w > 95\%$) may arise due to decrease in solubility of the probe **1** at higher water fraction ($f_w > 95\%$) resulting in more insoluble particles [20].

Probe **1** (20 μM) is found to be practically non-emissive in pure THF solution on exciting at 365 nm. However, as depicted from Figure 4, on progressive addition of water fraction to probe **1** in THF solution does not show any spectral change on the photoluminescence features up to $f_w = 90\%$, but an abrupt fluorescence

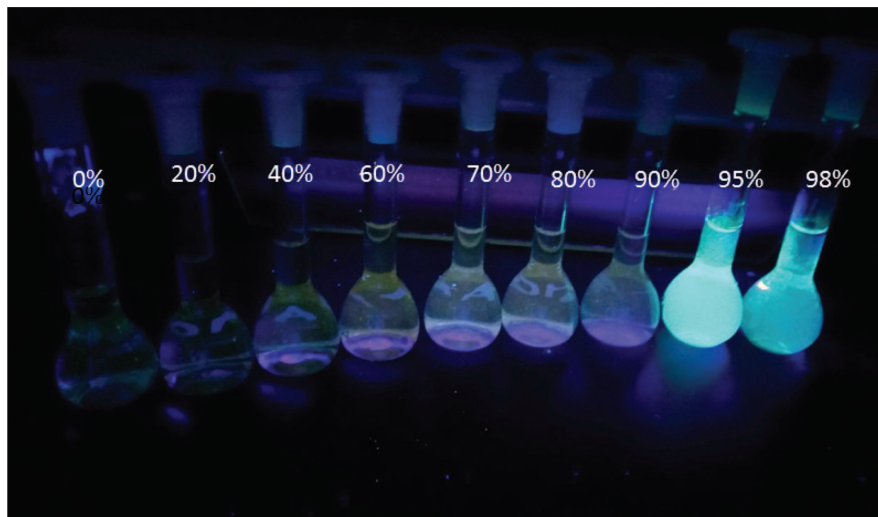


Fig. 2: Luminescent images of probe 1 in different water fraction ($fw = 0\text{--}98\%$) under 365 nm UV lamp.

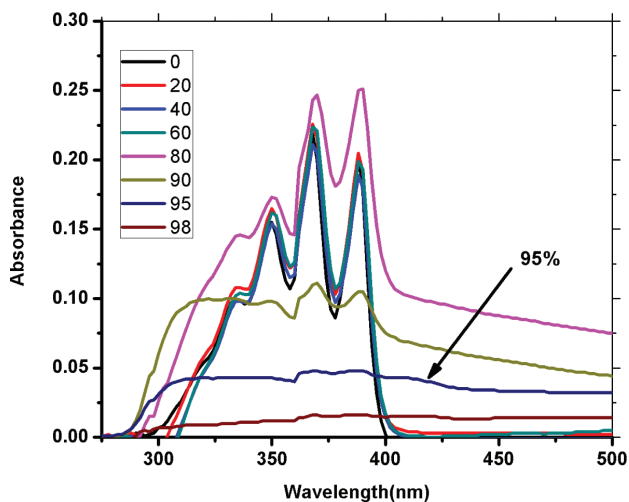


Fig. 3: Electronic absorption spectra of probe 1 (20 μM) in $\text{H}_2\text{O}/\text{THF}$ mixtures with different water fractions (fw).

amplification was observed with intense bright cyan emission at ~ 472 nm on reaching the water fraction of 95%. The emission intensity of at $fw = 95\%$ shows a 390-fold enhancement (expressed as $I - I_0/I_0$) in comparison with pure THF solution indicating a clear observation of aggregation induced emission (AIE) at this

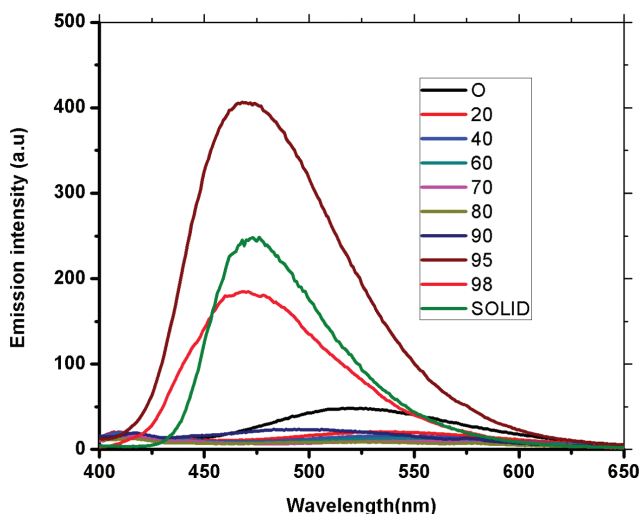


Fig. 4: Emission spectra of probe **1** (20 μM) in $\text{H}_2\text{O}/\text{THF}$ mixtures with different water fractions (f_w).

water fraction. The emission enhancement behavior of probe **1** at higher water fraction could be attributed to the formation of nanoaggregates that effectively suppress the intramolecular rotation and C=N imine bond isomerization effectively which in turn inhibit the non-radiative relaxation channels and activates radiative decay of the excited state molecule leading to aggregated state emission enhancement [21, 22]. It was found that addition of more water fraction ($f_w > 95\%$) results in dropping off the emission intensity; a characteristic phenomenon often observed with AIE luminogens. Though the reason for this phenomenon remains unclear, we speculate that the hydrophobic molecules of probe **1** adopt to aggregate into larger particles and precipitate rapidly at higher water fractions which may cause the decrease in the number of emitting molecules in the system and thus lowers fluorescence enhancement [23].

3.2 Colorimetric detection of metal ions

The interaction of metal ions with the probe **1** (20 μM) have been investigated at water fraction 95%. As seen in Figure 5, probe **1** shows visual color change from colorless to pale green upon addition of Cu^{2+} ions (10 equiv), whereas other metals ions such as Ag^+ , Co^{2+} , Ni^{2+} , Hg^{2+} , Zn^{2+} , Mn^{2+} , Cd^{2+} and Pb^{2+} did not display any significant visual change in color under similar experimental condition signifying the interesting feature of the probe molecule for to detect Cu^{2+} without any other instrumental support. The color change may arise due to the partly filled d

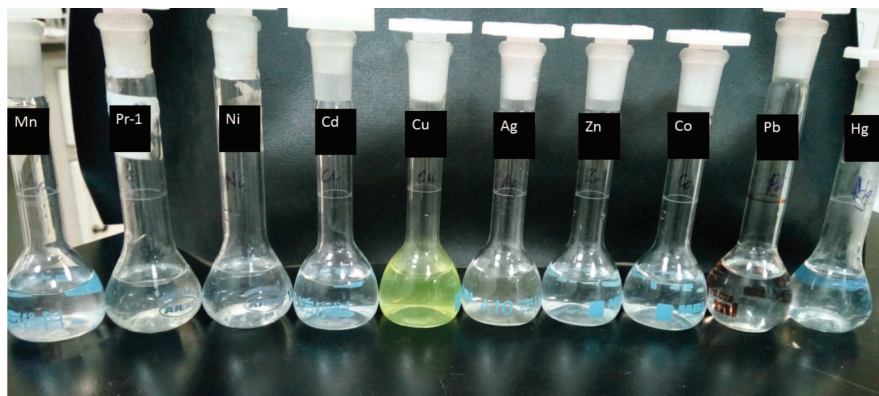


Fig. 5: Color changes of probe **1** (20 μM) after the addition respective metal ions (10 equiv.) in THF: H₂O mixtures, $f_w = 95\%$.

orbitals in Cu^{2+} ion where light is absorbed as electrons move from one d orbital to another [24].

3.3 Metal binding study

The sensing properties of probe **1** against various metal ions have been investigated by applying absorption and fluorescence spectral measurements in water/THF mixtures by keeping water fraction 95% to maintain the AIE behavior. At first, in order to check recognition abilities of probe **1** with different metal ions, metal binding test of probe **1** was evaluated using absorption measurements. The absorption profile of probe **1** was investigated upon addition of various metal ions (10 equiv) such as Ag^+ , Co^{2+} , Cu^{2+} , Ni^{2+} , Hg^{2+} , Zn^{2+} , Mn^{2+} , Cd^{2+} and Pb^{2+} in H₂O/THF ($f_w = 95\%$) solvent system. The effect of metal ions on probe **1** shows that the complex is much sensitive to Cu^{2+} ions by showing changes in the absorption band. As expected, coordination of Cu^{2+} to probe **1** resulted in the formation of red shifted broad absorption spectra at 473 nm with synchronous increase in the absorption band as seen Figure 6. The increase in absorption band of probe **1** on interaction with Cu^{2+} may be due to the ligand-to-metal charge transfer complex formation. Further, the interaction of Cu^{2+} with probe **1** has resulted with the disappearance of the structured band at 350–390 nm. It is interesting to note that other competitive cations did not show any obvious spectral changes suggesting the selectivity of probe **1** for Cu^{2+} in the presence of other metal ions.

The changes in emission intensity of probe **1** (20 μM) towards various metal ions was investigated by treating it with 10 equiv of varying metal ions namely

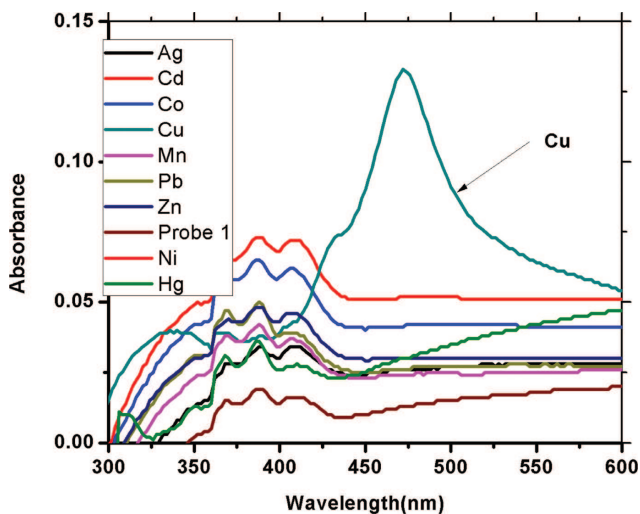


Fig. 6: Absorption spectra of probe 1 (20 μM) probe 1 upon addition of Ag^{1+} , Cd^{2+} , Co^{2+} , Cu^{2+} , Mn^{2+} , Pb^{2+} , Zn^{2+} , Hg^{2+} , Ni^{2+} and Ni^{2+} (10 equiv.) in THF: H_2O mixtures, $f_w = 95\%$.

Ag^+ , Co^{2+} , Cu^{2+} , Ni^{2+} , Hg^{2+} , Zn^{2+} , Mn^{2+} , Cd^{2+} and Pb^{2+} by keeping water fraction 95%. As seen from Figure 7, dramatic decrease in the emission spectra was observed on addition of ten equivalents Cu^{2+} ions, whereas no such changes

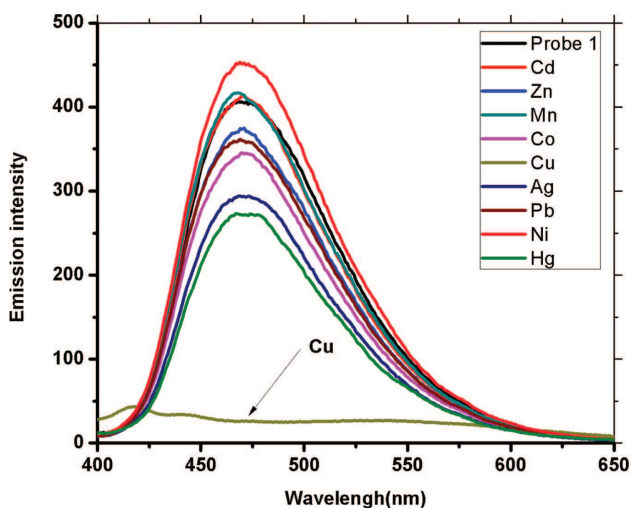


Fig. 7: Emission spectra of probe 1 (20 μM) probe 1 upon addition of Ag^{1+} , Cd^{2+} , Co^{2+} , Cu^{2+} , Mn^{2+} , Pb^{2+} , Zn^{2+} , Hg^{2+} , Ni^{2+} and Ni^{2+} (10 equiv.) in THF: H_2O mixtures, $f_w = 95\%$, ($\lambda_{\text{ex}} = 365 \text{ nm}$).

were observed with other metal ions. In case of Cu^{2+} , the emission intensity suffered significantly and resulted in almost quenching of fluorescence intensity compared to other tested metal ions which clearly demonstrates that probe **1** have higher selectivity towards Cu^{2+} ions over other tested metals. The observed quenching efficiency is found to be about 93.83% (expressed in $(I_0 - I)/I_0 \times 100$) by the addition Cu^{2+} as shown in Figure 8. The observed quenching of emission intensity by Cu^{2+} ions may be ascribed due to the paramagnetic nature of Cu^{2+} which result in chelation-enhanced quenching (CHEQ) by metal to ligand charge transfer reaction between probe **1** and Cu^{2+} [25].

Fluorescence titration experiment was carried out to have more insight into the sensing properties of probe **1** towards Cu^{2+} by changing the concentration of metal ions. As see in Figure 9, the intense fluorescence of probe **1** around 474 nm was gradually decreased on increasing the concentration of Cu^{2+} ions on exciting at 365 nm. In fact, treatment of even with 1 equiv of Cu^{2+} ions (20 μM) resulted in the quenching fluorescence effectively by 44% of the original value and almost 93% of quenching of emission intensity was obtained with 10 equiv of metal ions suggesting highly selective sensing ability of receptor **1** towards the detection of Cu^{2+} ions. Further, compared to other fluorescent probes that are available in the literature for Cu^{2+} sensing mostly work only in organic solvents whereas the probe **1** work in aqueous media for detection of copper ions as water is responsible for aggregation and a very low amount of probe (20 μM) is needed for quite efficient quenching.

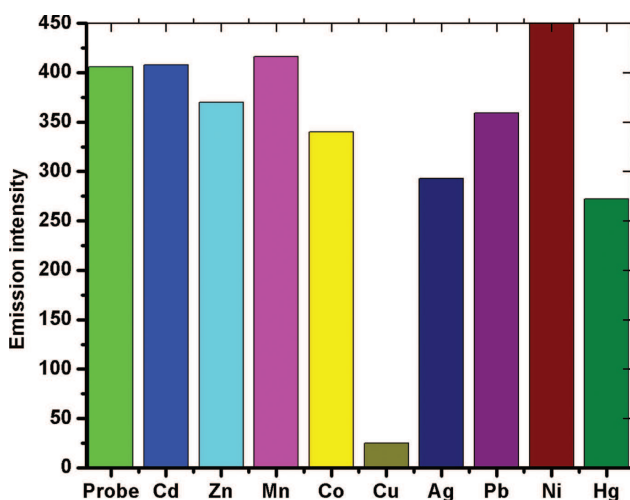


Fig. 8: Emission intensity of probe **1** in presence of different metal ions ($\lambda_{\text{ex}} = 365$ nm).

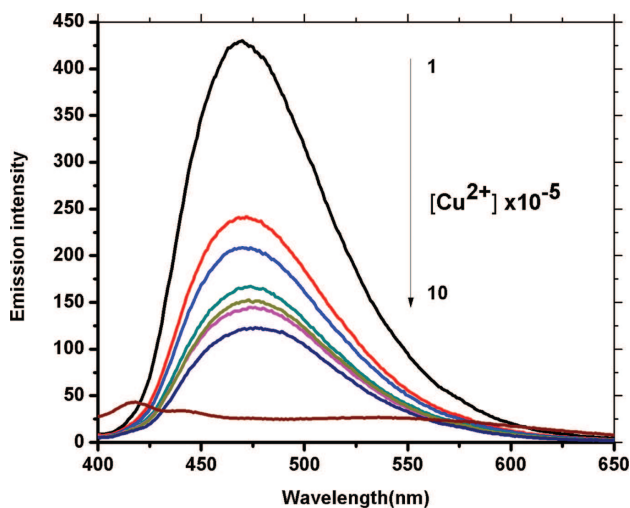


Fig. 9: PL spectra of probe **1** as a function of $[\text{Cu}^{2+}]$. $[\mathbf{1}] = 20 \mu\text{M}$ in THF:water mixtures, $f_{\text{W}} = 95\%$ ($\lambda_{\text{ex}} = 365 \text{ nm}$).

To gain insight into the nature of quenching mechanism and the extent of quenching, Stern-Volmer plot was constructed by applying Stern-Volmer equation [26],

$$\frac{I_0}{I} = 1 + K_{\text{SV}}[\text{Cu}]$$

where K_{SV} is the Stern–Volmer quenching constant, I_0 and I are the original fluorescence intensity and quenched intensity in presence of the quencher concentration $[\text{Cu}]$. The K_{SV} value obtained by plotting I_0/I values versus the concentrations of Cu^{2+} ions were found to be $2.4 \times 10^4 \text{ M}^{-1}$ with correlation coefficient (R^2) equal to 0.92 (Figure 10). The higher values for K_{SV} designate the efficient interaction between the Cu metal ions and fluorophore. The detection limit was calculated from fluorescence titration experiment, using the IUPAC definition i.e. $3\sigma/\text{slope}$ where σ is the standard deviation of 10 blank solutions of the sensor. The changes in the fluorescence intensity were recorded as a function of the change in concentration of Cu^{2+} ions. Detection limit calculated from the fluorescence titration data by varying the concentration of Cu^{2+} was found to be $2.14 \mu\text{M}$.

3.4 Computational details

The density functional theory (DFT) is found to be consistent to reproduce the experimental data. Moreover, it is reliable to predict various properties

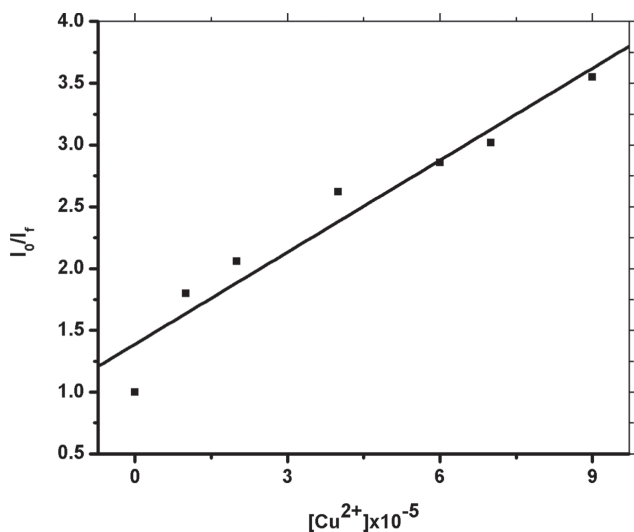


Fig. 10: Stern-Vollmer plot for probe 1 (20 μM) at various concentration of Cu^{2+} ions.

of interests. Previous studies showed that B3LYP is healthier choice to reproduce and predict the electronic properties [27–32]. Moreover, various semiconducting properties were studied by using B3LYP level [33, 34]. All calculations were executed with 6-31G** basis set except for Cu where LANL2DZ basis set was applied which was established accurate and rational for metal comprising compounds [35–37]. In the current study, ground state geometries of probe 1 and probe 1-Cu complex were optimized at B3LYP/6-31G** and B3LYP/6-31G** (LANL2DZ) level, respectively. Various properties of interests were calculated using Gaussian 09 package [27].

3.5 Binding energies

The binding energy ΔE of probe 1-Cu complex was estimated by using the following equation:

$$\Delta E = E(\text{AB}) - E(\text{A}) - E(\text{B})$$

where $E(\text{AB})$ is the energy of optimized probe 1-Cu complex whilst $E(\text{A})$ and $E(\text{B})$ are the optimized energies of probe 1 and Cu, respectively. The deprotonated hydrogen energy has also been added to probe 1-Cu complex to attain the reliable and accurate ΔE values. A positive ΔE value is specifying stable adsorption, see Table 1.

Tab. 1: The binding energies ΔE of probe 1-Cu complex computed at B3LYP/6-31G** and B3LYP/6-31G**(LANL2DZ) level.

Probe 1	-1032.7639686
Metal	-196.1168077
Reactant	-1228.880776
Complex	-1228.2889114
H	-0.50027
Product	-1228.789181
ΔE Kcal/mol	57.48

3.6 Electronic properties

As inferred from Figure 11, three frontier molecular orbitals (FMOs), highest occupied molecular orbital (HOMO) and unoccupied molecular orbitals (LUMO and LUMO+1) of probe 1 and its Cu-complexes have been showed. In probe 1, charge density of the HOMO and LUMO is distributed on anthracene moiety whereas LUMO+1 is localized at dihydroquinazolinone. The intra-molecular charge transfer (ICT) was found from anthracene of HOMO to dihydroquinazolinone unit (LUMO+1). In probe 1-Cu complex, most of the HOMO is distributed on dihydroquinazolinone with some charge density at anthracene. The LUMO is localized

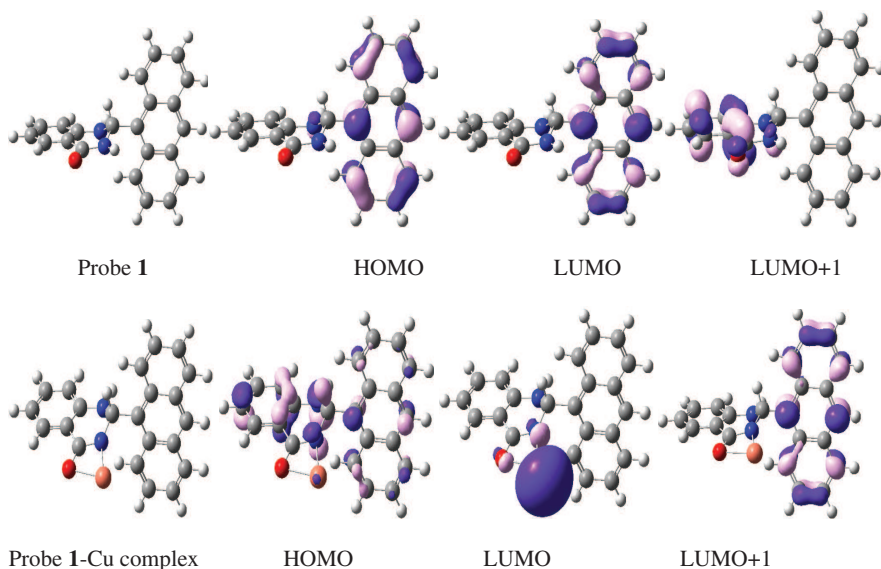


Fig. 11: Ground state frontier molecular orbitals of probe 1 and its Cu-complexes (contour value 0.05).

Tab. 2: The computed HOMO energies (E_{HOMO}), LUMO energies (E_{LUMO}), LUMO+1 energies ($E_{\text{LUMO}+1}$), HOMO-LUMO energy gap ($E_{\text{H-L}}$) and HOMO-LUMO+1 energy gap ($E_{\text{H-L}+1}$) for probe **1** at B3LYP/6-31G** and probe **1**-Cu complex at B3LYP/6-31G** (LANL2DZ) levels of theory.

Systems	E_{HOMO}	E_{LUMO}	$E_{\text{LUMO}+1}$	$E_{\text{H-L}}$	$E_{\text{H-L}+1}$
Probe 1	-5.51	-2.01	-0.89	3.50	4.62
Probe 1 -Cu complex	-5.27	-2.24	-1.78	3.03	3.49

on the Cu metal while LUMO+1 at anthracene moiety. The charge density distribution pattern on probe **1**-Cu complex is illuminating ligand to metal charge transfer (LMCT) from probe **1** (HOMO) to the metal ion (LUMO). This LMCT in probe **1**-Cu complex is playing important role to sense the Cu ions by probe **1**. In Table 2, we have displayed the calculated HOMO energies (E_{HOMO}), LUMO energies (E_{LUMO}), LUMO+1 energies ($E_{\text{LUMO}+1}$), HOMO-LUMO energy gap ($E_{\text{H-L}}$) and HOMO-LUMO+1 energy gap ($E_{\text{H-L}+1}$) for probe **1** at B3LYP/6-31G** and probe **1**-Cu complex at B3LYP/6-31G** (LANL2DZ) levels of theory. It can be observed that after binding the Cu ion to the probe **1** E_{HOMO} increases while E_{LUMO} and $E_{\text{LUMO}+1}$ decreases resulting reduced $E_{\text{H-L}}$ and $E_{\text{H-L}+1}$ in probe **1**-Cu complex as compared to the probe **1**. This reduced energy gap would be favorable in probe **1**-Cu complex to tune the absorption spectrum towards longer wavelength.

4 Conclusion

In summary, an anthracene appended dihydroquinazolinone derivative have been designed and synthesized. The solvent effect on the photophysical properties of probe molecule reveals that the emission profile is greatly influenced by the polarity of the solvents; suggesting involvement of photo induced intramolecular charge transfer (ICT) in the excited state. The AIE properties of the probe molecule has been elucidated using water/THF mixtures with different water volume fractions and found that the molecule emits strongly on reaching the water fraction 95%. Further, by exploiting the AIE property, the sensing ability of the probe molecule towards various metal ions unravel that it could act as a selective and sensitive sensor for Cu^{2+} ions through a turn-off fluorescence signaling mechanism as well as by colorimetric response. Theoretical studies further support intra-molecular charge transfer (ICT) from anthracene (HOMO) to dihydroquinazolinone unit (LUMO+1) in probe **1** where as in probe **1**-Cu complex ligand to metal charge transfer (LMCT) from probe **1** (HOMO) to the metal ion (LUMO) was noticed. Moreover, the decreased energy gap after binding the Cu ion to the probe **1** resulted

tuned the absorption of probe **1**-Cu complex towards longer wavelength. To conclude, the reported probe molecule enjoy greater practical interest as it works in aqueous media for detection of copper ions where the color change could be clearly observed by the naked eyes as well as the fluorescence changes imparted by the metal ion could be visualized with the help of a 365 nm UV lamp. Hence, the current direction of research will enhance the contribution to the global field of sensing technology by making cheap and efficient smart material to detect the heavy metal ions in solution and solid supported materials (test kits).

Acknowledgement: The authors extend their appreciation to the Deanship of Scientific Research at King Khalid University for funding this work through Research Group Project under grant number (R.G.P.1/15/38).

References

1. M. Ebrahimi, F. Rosei, *Nat. Photonics* **10** (2016) 434.
2. Y. Sagara, S. Yamane, M. Mitani, C. Weder, T. Kato, *Adv. Mater.* **28** (2016) 1073.
3. V. Mahendran, K. Pasumpon, S. Thimmarayaperumal, P. Thilagar, S. Shanmugam, *J. Org. Chem.* **81** (2016) 3597.
4. T. Han, X. Feng, D. Chen, Y. Dong, *J. Mater. Chem. C* **3** (2015) 7446.
5. S. Varughese *J. Mater. Chem. C* **2** (2014) 3499.
6. J. Cornil, D. Beljonne, J. P. Calbert, J. L. Bredas, *Adv. Mater.* **13** (2001) 1053.
7. M. I. Klimant, O. S. Wolfbeis, T. Werner, *Anal. Chim. Acta* **462** (2002) 1.
8. V. K. Gupta, A. K. Jain, G. Maheshwari, H. Langb, Z. Ishtaiwi, *Sens. Actuators B: Chem.* **117** (2006) 99.
9. Y. Gao, X. Li, M. J. Serpe, *RSC Adv.* **5** (2015) 44074.
10. A. Kavanagh, R. Byrne, D. Diamond, K. J. Fraser, *Membranes.* **2** (2012) 16.
11. X. Chen, T. Pradhan, F. Wang, J. S. Kim, J. Yoon, *Chem. Rev.* **112** (2011) 1910.
12. Y. Yang, Q. Zhao, W. Feng, F. Li, *Chem. Rev.* **113** (2012) 192.
13. S. Samanta, U. Manna, T. Ray, G. Das, *Dalton Trans.* **44** (2015) 18902.
14. R. Zhang, M. Gao, S. Bai, B. Liu, *J. Mater. Chem. B* **3** (2015) 1590.
15. M. Pannipara, A. G. Al-Sehemi, A. Kalam, A. M. Asiri, M. N. Arshad, *Spectrochim. Acta A Mol. Biomol. Spectrosc.* **183** (2017) 84.
16. R. Li, S. Xiao, Y. Li, Q. Lin, R. Zhang, J. Zhao, C. Yang, K. Zou, D. S. Li, T. Yi, *Chem. Sci.* **5** (2014) 3922.
17. F. Han, R. Zhang, Z. Zhang, J. Su, Z. Ni, *RSC Adv.* **6** (2016) 68178.
18. R. R. Hu, E. Lager, A. Aguilar-Aguilar, J. Z. Liu, J. W. Y. Lam, H. H. Y. Sung, I. D. Williams, Y. C. Zhong, K. S. Wong, C. E. Pena, B. Z. Tang, *J. Phys. Chem. C* **113** (2009) 15845.
19. B. Tang, Y. Geng, J. W. Y. Lam, B. Li, X. Jing, X. Wang, F. Wang, A. Pakhomov, X. Zhang, *Chem. Mater.* **11** (1999) 1581.
20. H. Auweter, H. Haberkorn, W. Heckmann, D. Horn, E. Lüddecke, J. Rieger, H. Weiss, *Angew. Chem. Int. Ed.* **38** (1999) 2188.

21. Y. Cao, M. Yang, Y. Wang, H. Zhou, Z. Jun, X. Zhang, J. Wu, Y. Tiana, Z. Wud, *J. Mater. Chem. C* **2** (2014) 3686.
22. A. Gogoi, S. Mukherjee, A. Ramesh, G. Das, *Anion Anal. Chem.* **87** (2015) 6974.
23. W. Fang, G. Zhang, J. Chen, L. Kong, L. Yang, H. Bi, J. Yang, *Sens. Actuators B Chem.* **229** (2016) 338.
24. D. Udhayakumari, S. Velmathi, P. Venkatesan, S.-P. Wu, *J Lumin.* **161** (2015) 411.
25. S. Zhang, Q. Niu, L. Lan, T. Li, *Sens. Actuators B Chem.* **240** (2017) 793.
26. J. R. Lakowicz, *Principles of Fluorescence Spectroscopy*, third ed., Springer, New York (2006).
27. M. J. Frisch, G. W. Trucks, H. B. Schlegel, G. E. Scuseria, M. A. Robb, J. R. Cheeseman, G. Scalmani, V. Barone, B. Mennucci, G. A. Petersson, H. Nakatsuji, M. Caricato, X. Li, H. P. Hratchian, A. F. Izmaylov, J. Bloino, G. Zheng, J. L. Sonnenberg, M. Hada, M. Ehara, K. Toyota, R. Fukuda, J. Hasegawa, M. Ishida, T. Nakajima, Y. Honda, O. Kitao, H. Nakai, T. Vreven, J. A. Montgomery Jr, J. E. Peralta, F. Ogliaro, M. Bearpark, J. J. Heyd, E. Brothers, K. N. Kudin, V. N. Staroverov, R. Kobayashi, J. Normand, K. Raghavachari, A. Rendell, J. C. Burant, S. S. Iyengar, J. Tomasi, M. Cossi, N. Rega, J. M. Millam, M. Klene, J. E. Knox, J. B. Cross, V. Bakken, C. Adamo, J. Jaramillo, R. Gomperts, R. E. Stratmann, O. Yazyev, A. J. Austin, R. Cammi, C. Pomelli, J. W. Ochterski, R. L. Martin, K. Morokuma, V. G. Zakrzewski, G. A. Voth, P. Salvador, J. J. Dannenberg, S. Dapprich, A. D. Daniels, Ö. Farkas, J. B. Foresman, J. V. Ortiz, J. Cioslowski, D. J. Fox, *Gaussian-09, Revision A.1*, Gaussian, Inc., Wallingford, CT (2009).
28. W. Kohn, A. D. Becke, R. G. Parr, *J. Phys. Chem.* **100** (1996) 12974.
29. A. D. Becke, *J. Chem. Phys.* **98** (1993) 5648.
30. R. S. Sánchez-Carrera, V. Coropceanu, D. A. da Silva Filho, R. Friedlein, W. Osikowicz, R. Murdey, C. Suess, W. R. Salaneck, J.-L. Brédas, *J. Phys. Chem. B* **110** (2006) 18904.
31. A. Irfan, S. Muhammad, A. R. Chaudhry, A. G. Al-Sehemi, R. Jin, *Optik – Intern. J. Light Elect. Optics.* **149** (2017) 321.
32. D. Guillaumont, S. Nakamura, *Dyes Pigm.* **46** (2000) 85.
33. A. Irfan, A. G. Al-Sehemi, A. R. Chaudhry, S. Muhammad, *Optik – Intern. J. Light Elect. Optics.* **138** (2017) 349.
34. A. Irfan, A. G. Al-Sehemi, A. R. Chaudhry, S. Muhammad, *J. King Saud Uni. – Sci.* **30** (2018) 458.
35. Y. Yang, M. N. Weaver, K. M. Merz, *J. Phys. Chem. A* **113** (2009) 9843.
36. G. Abbas, A. Hassan, A. Irfan, M. Mir, G. Wu, *J. Struct. Chem.* **56** (2015) 92.
37. A. Irfan, J. Zhang, Y. Chang, *Chem. Phys. Lett.* **483** (2009) 143.